Chromatin accessibility landscapes activated by cell-surface and intracellular immune receptors

Ding, P.; Sakai, T.; Krishna, S.R.; Manosalva, P.N.; Guo, W.; Ngou, B.P.K.; ... ; Jones, J.D.G.

Journal of Experimental Botany, Vol. 72, No. 22 pp. 7927–7941, 2021
https://doi.org/10.1093/jxb/erab373 Advance Access Publication 13 August 2021

RESEARCH PAPER

Chromatin accessibility landscapes activated by cell-surface and intracellular immune receptors

Pingtao Ding[1,*,†], Toshiyuki Sakai[1], Ram Krishna Shrestha[1], Nicolas Manosalva Perez[2,3], Wenbin Guo[4], Bruno Pok Man Ngou[1], Shengbo He[5], Chang Liu[6], Xiaoqi Feng[5], Runxuan Zhang[4], Klaas Vandepoele[2,3], Dan MacLean[1], and Jonathan D.G. Jones[1,*]

[1] The Sainsbury Laboratory, University of East Anglia, Norwich Research Park, Norwich NR4 7UH, UK
[2] Department of Plant Biotechnology and Bioinformatics, Ghent University, Technologiepark 71, 9052 Ghent, Belgium
[3] VIB Center for Plant Systems Biology, Technologiepark 71, 9052 Ghent, Belgium
[4] Information and Computational Sciences, The James Hutton Institute, Dundee DD2 5DA, UK
[5] John Innes Centre, Norwich Research Park, Norwich NR4 7UH, UK
[6] Institute of Biology, University of Hohenheim, Garbenstrasse 30, 70599 Stuttgart, Germany

[†] Current address: Institute of Biology Leiden, Leiden University, Sylviusweg 72, Leiden 2333 BE, The Netherlands
*Correspondence: p.ding@biology.leidenuniv.nl or jonathan.jones@tsl.ac.uk

Received 11 September 2020; Editorial decision 3 July 2021; Accepted 12 August 2021

Editor: John Lunn, MPI of Molecular Plant Physiology, Germany

Abstract

Activation of cell-surface and intracellular receptor-mediated immunity results in rapid transcriptional reprogramming that underpins disease resistance. However, the mechanisms by which co-activation of both immune systems lead to transcriptional changes are not clear. Here, we combine RNA-seq and ATAC-seq to define changes in gene expression and chromatin accessibility. Activation of cell-surface or intracellular receptor-mediated immunity, or both, increases chromatin accessibility at induced defence genes. Analysis of ATAC-seq and RNA-seq data combined with publicly available information on transcription factor DNA-binding motifs enabled comparison of individual gene regulatory networks activated by cell-surface or intracellular receptor-mediated immunity, or by both. These results and analyses reveal overlapping and conserved transcriptional regulatory mechanisms between the two immune systems.

Keywords: ATAC-seq and RNA-seq, cell surface immune receptors, chromatin accessibility, gene regulatory network, intracellular immune receptors, plant innate immunity, PRR and NLR, transcriptional regulation.

Introduction

Plants use both cell-surface and intracellular receptors to detect pathogen-derived molecules and activate innate immunity (Jones and Dangl, 2006). Plant cell-surface immune receptors (pattern recognition receptors, or PRRs) perceive relatively conserved pathogen-associated molecular patterns (PAMPs) or endogenous damage-associated molecular patterns (DAMPs) released from damaged or dying plant cells, and activate PAMP-triggered immunity (PTI) or

DAMP-triggered immunity (Choi and Klessig, 2016; Bacete *et al.*, 2018). Intracellular immune receptors in plants are usually nucleotide-binding, leucine-rich repeat (NLR) proteins. NLRs recognize, directly or indirectly, pathogen effectors secreted into plant cells and activate effector-triggered immunity (ETI). These innate immune systems involve distinct responses mediated by different subsets of molecular components (Ngou *et al.*, 2021). Some cell-surface receptors, such as tomato Cf-4 and Cf-9, detect apoplastic effectors yet activate both PTI-like and ETI-like responses (Hammond-Kosack and Jones, 1997). The main fundamental distinction is between processes initiated by cell-surface or intracellular immune receptors (Supplementary Fig. S1). In interactions between plants and microbial pathogens, PTI will always precede ETI, because effector delivery requires intimate host–microbe contact.

We used the Arabidopsis RPS4/RRS1 NLR pair as a model to study ETI, which detects the bacterial effectors AvrRps4 and PopP2. Using a *Pseudomonas* strain that delivers only one of these effectors, we defined early RPS4/RRS1-dependent transcriptional responses in Arabidopsis leaves (Sohn *et al.*, 2014; Ding *et al.*, 2020), and showed that 4 h after infiltration, PTI together with ETI ('PTI+ETI') elevates the expression of defence-related genes more strongly than PTI alone (Sohn *et al.*, 2014; Ding *et al.*, 2020). This early time-point precedes the accumulation of the defence hormone salicylic acid (SA) and gene reprogramming in response to an increased endogenous SA level (Sohn *et al.*, 2014; Ding *et al.*, 2020). This implies that ETI-enhanced transcriptional regulation plays an essential role in conferring robust immune responses against pathogens (Ngou *et al.*, 2021), but how ETI activates defence genes remains unclear. To study ETI-specific physiological changes, we generated an inducible ETI system (Ngou *et al.*, 2020).

The activation of PTI, ETI, and 'PTI+ETI' leads to rapid transcriptional reprogramming (Sohn *et al.*, 2014; Hillmer *et al.*, 2017; Ding *et al.*, 2020). Many transcriptional regulatory components are known to be involved in orchestrating effective immunity in plants (Tsuda and Somssich, 2015; Li *et al.*, 2016), notably transcription factors (TFs) (Zhang *et al.*, 2010), transcription co-repressors (Zhu *et al.*, 2010), the Mediator complex (Kidd *et al.*, 2009), histone-modifying enzymes (Zhou *et al.*, 2005), and histone remodellers (Walley *et al.*, 2008). Little is known about how changes in the rates of transcription of defence genes are initiated, maintained, and regulated upon the activation of either class of plant immune receptor.

Open accessible chromatin regions (ACRs) at promoters and enhancers are associated with active gene expression in eukaryotes (Tsompana and Buck, 2014). DNA methylation, histone deacetylation, and histone methylation can prime the promoters of immune-related genes required for disease defence (Chen *et al.*, 2017). Conversion between 'closed' and 'open' chromatin states results from chromatin remodelling, which is regulated by multi-unit complexes. Several putative chromatin remodellers play important roles in regulating defence gene expression during the activation of PTI and ETI, including the SWI/SNF chromatin remodeller SYD (SPLAYED) (Johnson *et al.*, 2015), the SWR1c subunits PHOTOPERIOD-INDEPENDENT EARLY FLOWERING1 (PIE1), ACTIN-RELATED PROTEIN6 (ARP6), and SWR1 COMPLEX 6 (SWC6), as well as H2A.Z (Berriri *et al.*, 2016), and the CHROMATIN-REMODELING FACTOR 5 (CHR5) (Zou *et al.*, 2017). However, the detailed profiling of chromatin status induced by PTI, ETI, or 'PTI+ETI' has never been reported before, and the direct association between the changes in the chromatin status and the changes in defence gene expression is unclear.

The application of assays for transposase-accessible chromatin followed by sequencing (ATAC-seq) in plants has revealed species-, tissue-, and cell-type-specific chromatin signatures in recent studies (Lu et al., 2017, 2019; Maher *et al.*, 2018; Potter *et al.*, 2018; Frerichs *et al.*, 2019), but changes in chromatin accessibility associated with inducible responses and environmental perturbations, such as immune activation, are less well characterized. We hypothesized that correlating immunity-specific transcriptomes with an atlas of open chromatin profiles would reveal *cis*-regulatory elements and associated regulatory mechanisms that underpin these changes. We therefore performed a set of comparative analyses with ATAC-seq and RNA sequencing (RNA-seq) data generated during PTI, 'PTI+ETI', and ETI. This study provides an extensive data resource for the plant–microbe interaction community, which demonstrates a direct link between changes in chromatin accessibility and associated gene expression and new insights into the dynamics of chromatin accessibility landscapes and gene regulatory networks (GRNs) during plant immune activation.

Materials and methods

Plant materials and growth conditions

Arabidopsis thaliana Columbia-0 (Col-0) accession was used as the wild type in this study. The SETI^{WT} and SETI^{mut} transgenic plants used have been described previously (Ngou *et al.*, 2020). Seeds were sown on compost and plants were grown at 21 °C with 10-h light/14-h darkness and at 70% humidity. The light level was approximately 180–200 μmol, provided by fluorescent tubes.

Activation of PTI and 'PTI+ETI'

Pseudomonas fluorescens engineered with a type III secretion system (Pf0-1 'EtHAn' strains) expressing one of wild-type AvrRps4 or AvrRps4 KRVY135-138AAAA mutant effectors were grown on selective KB plates for 24 h at 28 °C (Thomas *et al.*, 2009; Sohn *et al.*, 2014). Bacteria were harvested from the plates and resuspended in infiltration buffer (10 mM $MgCl_2$), and the concentration was adjusted to OD_{600}=0.2 (10^8 CFU ml^{-1}). The abaxial surfaces of 5-week-old Arabidopsis fully expanded leaves were hand infiltrated with a 1 ml disposable needleless syringe (Slaughter Ltd, R & L, catalogue number: BS01T). Leaves infiltrated with 10 mM $MgCl_2$ served as mock treatment. Leaves infiltrated with Pf0-1:AvrRps4^{WT} activate 'PTI+ETI', and those infiltrated with Pf0-1:AvrRps4^{mut} activate PTI only (Ngou *et al.*, 2021).

Activation of ETI

Leaves of 5-week-old Arabidopsis of SETI^{WT} (E2:AvrRps4^{WT}) infiltrated with 50 μM β-estradiol (E2, Sigma-Aldrich, catalogue number: E8875; dissolved in 100% DMSO, Sigma-Aldrich, catalogue number: D8418) activate ETI only, as described previously(Ngou *et al.*, 2020). DMSO at a dilution of 0.1% (same titrate as 50 mM E2 stock solution diluted in pure water and generating 50 μM E2 working solution) in pure water was used as mock treatment for infiltration with a 1 ml needleless syringe. SETI^{mut} (E2:AvrRps4^{mut}) leaves with similar treatments as those applied to SETI^{WT} were used as additional negative ETI controls, as described previously (Ngou *et al.*, 2020).

RNA isolation and sequencing

Leaf samples from PTI, 'PTI+ETI', and ETI conditions were isolated as described previously (Ding *et al.*, 2020). Total RNA samples were sent, packed in dry ice, to BGI for mRNA isolation and library construction, and were sequenced on BGISEQ-500 sequencing platforms.

RNA-seq raw data processing, alignment, quantification of expression, and data visualization

Raw reads were trimmed into 50 bp clean reads by the BGI bioinformatics service. At least 12 million single-end clean reads for each sample were provided by BGI for RNA-seq analysis. All reads passed FastQC before the following analyses (FastQC: https://www.bioinformatics.babraham.ac.uk/projects/fastqc/). All clean reads were mapped either to the TAIR10 Arabidopsis genome/transcriptome via TopHat2 or to a comprehensive Reference Transcript Dataset for Arabidopsis (AtRTD2) containing 82 190 non-redundant transcripts from 34 212 genes via Kallisto (PTI and 'PTI+ETI') or Salmon (ETI) tools (Kim *et al.*, 2013; Bray *et al.*, 2016; Patro *et al.*, 2017; Zhang *et al.*, 2017). Detailed scripts and versions of each software can be found on GitHub at: https://github.com/TeamMacLean/fastqc_kallisto_analysis. Mapped reads were sorted with SAMtools and visualized in Integrative Genomics Viewer (IGV) with the TAIR10 reference genome (Li *et al.*, 2009; Robinson *et al.*, 2011; Kim *et al.*, 2013). The estimated gene transcript counts were used for differential gene expression analysis and statistical analysis with the 3D RNA-seq software (Guo *et al.*, 2020). For both datasets, the low expressed transcripts were filtered if they did not meet the criteria ≥3 samples with ≥1 count per million reads. An expressed gene must have at least one expressed transcript. The batch effects between biological replicates were removed to reduce artificial variance with the RUVSeq method (Risso *et al.*, 2014). The expression data were normalized across samples with the TMM method (Robinson and Oshlack, 2010). The significance of expression changes in the contrasting groups 'PTI vs no treatment' and 'PTI+ETI vs no treatment', and 'ETI vs Control_1' and 'ETI vs ETI_mut', were determined by the limma-voom method (Law *et al.*, 2014; Ritchie *et al.*, 2015). A gene was defined as a significant differentially expressed gene (DEG) if it had a Benjamini–Hochberg adjusted *P*-value <0.01 and $\log_2$[fold_change (FC)] ≥1.

FANS-ATAC-seq

Leaf samples from PTI, 'PTI+ETI', ETI and control conditions were collected at 4 h post-infiltration (hpi) of treatment (at the same time point as the RNA-seq samples) or without any treatment. Two fully expanded leaves with the same treatment from the same plant were collected, and in total six leaves from three plants with the same treatment were counted as one sample (one biological replicate). Six leaves of one sample were chopped quickly (<1 min) in 1 ml pre-chilled (4 °C) 1× phosphate-buffered saline (PBS) buffer (pH 7.4) with a clean unused razor blade (Agar Scientific Ltd, catalogue number: T586) into fine pieces. The leaf lysis, containing crude nuclei extract, was transferred and filtered through a 30 μm CellTrics® cell strainer (Sysmex, catalogue number: 04-0042-2316) into a 100×16 mm round-base test tube (Slaughter Ltd, R & L, catalogue number: 142AS) by pipetting a with 1 ml sterile tip. The sharp end of the tip was cut off and shortened by 2 mm with a pair of sterile scissors to minimize damage to the nuclei. All leaf lysis samples were kept on ice immediately after transfer. A 1 ml volume of CyStain propidium iodide Absolute P nuclei staining buffer (Sysmex, catalogue number: 05-5022) was added to each nuclei extract, and the extracts with the staining buffer were gently mixed and kept on ice. Stained nuclei extracts were submitted to fluorescence-assisted nuclei sorting (FANS) performed on a BD FACSMelody Cell Sorter with a green laser, with similar settings as described previously (Lu *et al.*, 2017). FANS-purified nuclei samples were collected in 1.5 ml DNA LoBind Eppendorf microcentrifuge tubes (Fisher Scientific, catalogue number: 10051232) and kept on ice. Pellets of nuclei were collected as described previously by centrifugation at 1000× *g* and tagmented with a Nextera DNA Library Prep Kit (Illumina, catalogue number: FC-121-1030, now discontinued; replacement can be found as Illumina Tagment DNA TDE1 Enzyme and Buffer Kits, catalogue numbers: 20034197 or 20034198) (Buenrostro *et al.*, 2015). We used 0.1 μl TDE1 enzyme in a 5 μl total reaction mix for each ATAC sample. PCR library construction and quality control steps were performed as recommended by Buenrostro *et al.* (2015); the only difference here was that we used dual index primers designed by ourselves for barcoding the libraries and multiplexing. Those primers have been validated in our previous experiments (Ding *et al.*, 2020), and the detailed sequence information can be found in Supplementary Table S1. Multiplexed ATAC-seq libraries were sequenced with multiple NextSeq 500/550 High Output Kits (75 cycles) on an in-house NextSeq 550 sequencer.

ATAC-seq raw data processing and alignment

Sequencing results were demultiplexed using the bcl2fastq tool to generate adaptor-trimmed raw reads. Paired-end and 37 bp each end reads were tested with FastQC and Picard tools for quality control and for testing PCR duplications. Raw reads were mapped to the TAIR10 Arabidopsis reference genome with Bowtie2 and sorted with SAMtools (Li *et al.*, 2009; Langmead and Salzberg, 2012). Reads mapped to chloroplasts and mitochondria were removed before the follow-up analyses. Detailed scripts, software versions, and QC outputs can be found on GitHub at: https://github.com/TeamMacLean/dingp_atacseq_for_publication.

Identification of ACRs

Identification of ACRs was done by the callpeak function in MACS v.2.2.7 (Zhang *et al.*, 2008). All replicates of samples under specific conditions were used as the input of treatment and genomic DNA samples were used as the input of control. For visualization of fold enrichment of mapped reads compared with control samples, FE.bdg files were generated by the bdgcmp function in MACS. FE.bdg files were visualized by IGV (Robinson *et al.*, 2011). In the trial analysis of FANS-ATAC-seq, we counted mapped reads for ACRs using the coverage function in Bedtools v.2.28.0 (Quinlan and Hall, 2010). Then, we made correlation plots based on $\log_2$ read counts of each common ACR between replicates to find out the reproducibility for 10 000 (10k), 20k, 50k, and 80k samples using our R script, which is listed on GitHub at: https://github.com/slt666666/Plant_Innate_Immunity_ATAC-seq.

Profile of ACRs binding to TSS/TTS regions

The heatmap of ACRs binding to transcription start site (TSS) regions and the distribution of ACRs binding to TSS and transcription

termination site (TTS) regions were obtained by the ChIPSeeker v.1.24.0 package in R (Yu *et al.*, 2015). The features of ACRs were annotated by the ChIPSeeker package using the annotatePeak function. In this part, promoters were defined as –2000 bp to 1000 bp from the TSS. The Upset plots, which showed ACRs shared in several conditions, were generated by the UpSetR package based on the nearest genes from ACRs (Conway *et al.*, 2017).

Identification of DARs

Identification of differentially accessible regions (DARs) was achieved by applying the callpeak function of MACS. All replicates of samples under a specific condition were used as the input of treatment and all replicates of samples under the corresponding control conditions were used as the input of control. Annotation of genes with enriched DARs within 2 kb upstream of a gene was done by the annotatePeakInBatch function in the ChIPpeakAnno package (Yu *et al.*, 2015). Annotation of genes with other DARs in distal intergenic genome loci was done by our Python script.

Integration of DEGs and DARs

The identification of genes common to the annotated genes with enriched DARs and the significantly up-regulated ($\log_2$FC>1, q-value<0.01) genes was done by our Python script. Gene ontology (GO) analysis for these common genes is conducted by using g:Profiler (Raudvere *et al.*, 2019). All scripts used for the analyses of ACRs and the integration of DEGs and DARs are available on GitHub at: https://github.com/slt666666/Plant_Innate_Immunity_ATAC-seq.

Motif-based inference of GRNs using ACRs

The inference of GRNs was done using an ensemble motif mapping method described previously (Kulkarni *et al.*, 2019), combining all the matches from Find Individual Motif Occurrences (FIMO) with the top 7000 matches from Cluster-Buster (CB) (Frith *et al.*, 2003; Grant *et al.*, 2011). This mapping information was used to determine which motifs were significantly enriched in the ACRs derived from the ATAC-seq experiments for each condition (PTI, ETI, and 'PTI+ETI'). Per condition, for TFs showing differential expression, the associated motifs were tested for enrichment in the ACRs and significant motifs were retained (adjusted P-value≤0.01). Based on motif coordinates in ACRs, individual motif matches were assigned to the closest gene, establishing a link between the TFs that bind these motifs and putative target genes. The differential expression information was integrated to identify only the TFs and target genes that were differentially expressed for each condition. Finally, for each TF, the putative target gene set was analysed for over-represented GO Biological Process terms (only using experimentally and curated annotations; hypergeometric distribution q-value<0.001).

Results

ATAC-seq in Arabidopsis reveals tissue-specific chromatin accessibility

ATAC-seq was first used to capture open chromatin regions in human cell lines and was rapidly adapted to other eukaryotic systems, including plants (Buenrostro *et al.*, 2013; Lu *et al.*, 2017). To study the dynamic chromatin features during plant immune activation, we established a protocol to prepare fresh nuclei isolated from adult rosette leaves of Arabidopsis Col-0 ecotype using FANS (Supplementary Fig. S2A). A similar approach was reported previously (Lu *et al.*, 2017). To generate FANS-ATAC-seq libraries from multiple samples that are (i) compatible with the Illumina next-generation sequencing platforms and (ii) can be multiplexed, we designed and synthesized barcoded primers with 9 nt unique indices for dual index and paired-end sequencing (Supplementary Fig. S2B–D, Supplementary Table S1). In a trial run, we used 10k, 20k, 50k, and 80k sorted nuclei as ATAC input with a fixed amount of 'tagmentation' reaction, to obtain an optimal ratio between the input nuclei (DNA) and Tn5 transposase (Supplementary Fig. S3A). Purified naked Arabidopsis genomic DNA was tagmented in three replicates and sequenced as controls for ATAC-seq normalization (Supplementary Fig. S2D). In this trial FANS-ATAC-seq run, we observed reproducible accessible chromatin features captured in two biological replicates with different levels of input (Supplementary Fig. S3B–E).

To test whether this ATAC-seq method is sensitive enough to detect tissue-specific chromatin accessible features, we additionally performed FANS-ATAC-seq with sperm nuclei and vegetative nuclei, the male germ unit derived from Arabidopsis pollen grain. We found that ACRs enriched at the *SYSTEMIC ACQUIRED RESISTANCE DEFICIENT 1* (*SARD1*) defence gene locus are observed only in somatic cells and not in germline cells (Supplementary Fig. S4A). *SARD1* encodes a TF involved in plant immunity (Zhang *et al.*, 2010; Wang *et al.*, 2011; Sun *et al.*, 2015). We inspected another well-known *Resistance* (*R*)-gene cluster on Arabidopsis chromosome 4, which harbours a group of N-terminal Toll/interleukin-1 receptor/resistance protein (TIR) domain-containing NLRs. Similar to *SARD1*, promoters of the NLR-encoding genes *RECOGNITION OF PERONOSPORA PARASITICA 4* (*RPP4*) or *CHILLING SENSITIVE 2* (*CHS2*), *SUPPRESSOR OF NPR1-1, CONSTITUTIVE 1* (*SNC1*), *SIDEKICK SNC1 1* (*SIKIC2*), and *RESISTANCE TO LEPTOSPHAERIA MACULANS 3* (*RLM3*) show enriched ACRs in leaf nuclei ATAC-seq data compared with the other four NLR-encoding genes in the same gene cluster, but not in the sperm nuclei or vegetative nuclei ATAC-seq data (Supplementary Fig. S4B). This is consistent with the observation that the expression levels of *RPP4/CHS2*, *SNC1*, *SIKIC2*, and *RLM3* in Arabidopsis adult leaves are much higher than those of the other four NLR-encoding genes in the same gene cluster (Schmid *et al.*, 2005). Expression of *RPP4/CHS2*, *SNC1*, *SIKIC2*, and *RLM3* in Arabidopsis leaves contributes to resistance against multiple pathogens (van der Biezen *et al.*, 2002; Zhang *et al.*, 2003; Staal *et al.*, 2008; Dong *et al.*, 2018; Asai *et al.*, 2018). In addition, trimethylation of the fourth lysine of histone H3 (H3K4me3s), a histone marks that is often associated with actively transcribed genes, is enriched in the *RPP4/CHS2* and *SNC1* promoters in Arabidopsis (Xia *et al.*, 2013), supporting our ATAC-seq results (Supplementary Fig. S4B). Overall, ACRs enriched in immunity-related genes are specific to somatic cells but not to germline cells.

ATAC-seq to study Arabidopsis inducible innate immunity

We applied the FANS-ATAC-seq method to study changes in chromatin accessibility associated with gene expression induced by innate immunity. In Arabidopsis Col-0, two paired NLR proteins, RPS4/RRS1 and RPS4B/RRS1B, serve as intracellular NLR receptors activating ETI upon recognition of AvrRps4, an effector derived from *Pseudomonas syringae* pv. *pisi*, a causal agent of bacterial blight in pea (*Pisum sativum*) (Saucet *et al.*, 2015). We used a non-pathogenic strain of *P. fluorescens* Pf0-1 engineered with the type III secretion system (T3SS) from *P. syringae* ('Effector-to-Host Analyzer' or EtHAn) as a tool to deliver wild-type AvrRps4 (Pf0-1:AvrRps4^{WT}) or its mutant (Pf0-1:AvrRps4^{mut}) into Col-0 leaf cells (Sohn *et al.*, 2009; Thomas *et al.*, 2009). AvrRps4^{mut} (KRVY135-138AAAA) is unable to activate ETI mediated by RPS4/RRS1 and RPS4B/RRS1B (Saucet *et al.*, 2015). Infiltration of Pf0-1:AvrRps4^{mut} activates PTI, and infiltration of Pf0-1:AvrRps4^{WT} activates 'PTI+ETI' (Supplementary Fig. S5A), as in previous reports (Ding *et al.*, 2020; Ngou *et al.*, 2021). We took samples at 4 hpi for ATAC-seq to monitor early changes during immune activation (Supplementary Fig. S5A) (Sohn *et al.*, 2014; Ding *et al.*, 2020). We obtained similar patterns of genome-wide ATAC-seq peak coverage with different treatments (Supplementary Fig. S5B).

ATAC-seq peaks in all biological replicates under different conditions were enriched within 2 kb upstream of the TSS and within 1 kb downstream of the TTS (Fig. 1A, B). The distribution of ACRs relative to genomic features was highly similar between all ATAC-seq datasets (Supplementary Fig. S5C–F, Supplementary Table S2). Over 77% of ACRs were mapped to the putative gene promoters (pACRs; within 2 kb upstream of a gene) (Supplementary Fig. S5C–F), consistent with previously reported ATAC-seq datasets (Lu *et al.*, 2017; Sijacic *et al.*, 2018). Approximately 8% of ACRs mapped to distal intergenic genome loci (dACRs) (Supplementary Fig. S5C–F), slightly higher than the 5.9% reported recently (Lu *et al.*, 2019). In addition, compared with the 16 296 ACRs observed in total using a similar FANS-ATAC-seq approach in a recent report (Lu *et al.*, 2019), we obtained a range of 24 901–27 285 total ACRs (Fig. 1C, Supplementary Table S3), also slightly more than the 23 288 total reported elsewhere applying ATAC-seq with INTACT (isolation of nuclei tagged in specific cell types)-purified nuclei (Maher *et al.*, 2018). Comparing ACRs enriched in all conditions, we found that 10 658 (~40% of total ACRs) were shared (Fig. 1C). The remaining 60% unshared ACRs may point to regulatory signals that are specific to each condition.

Among the shared ACRs, pACRs enriched at housekeeping gene loci, such as *UBQ10* (*POLYUBIQUITIN 10*), showed similar patterns in all conditions (Fig. 1D), consistent with the presumed constitutive expression. pACRs enriched at *SNC1* and *SARD1* were similar to those observed in our trial run (Supplementary Fig. S4) and the major peaks of pACRs at these two gene loci under different conditions were similar. We observed additional small pACRs at *SNC1* and increased ACRs at the 3′UTR of *SARD1* upon the PTI and 'PTI+ETI' treatments (Fig. 1E, F). These observations are positively correlated with previous reports that the expression of *SARD1* and *SNC1* is up-regulated by immune activation (Xia *et al.*, 2013; Ding *et al.*, 2020).

Positive correlation of increased ACRs and expression of defence genes during PTI and 'PTI+ETI'

We previously reported that some defence genes are induced by both PTI and 'PTI+ETI' by profiling the expression of selected genes (Ding *et al.*, 2020). In this study, we performed genome-wide RNA-seq to study genes induced by PTI and 'PTI+ETI' more extensively (Supplementary Fig. S6A, B). There were 4665 and 5004 up-regulated genes during PTI and 'PTI+ETI' compared to the 'No treatment' control, respectively. Among these, 4494 genes were shared by PTI and 'PTI+ETI' (Supplementary Fig. S6C, Supplementary Table S4). Similarly, there were 5433 down-regulated genes shared by PTI and 'PTI+ETI' (Supplementary Fig. S6C). This greatly expands the list shared of genes showing similar regulatory patterns between PTI and 'PTI+ETI' compared with our previous report (Supplementary Fig. S6C, D, Supplementary Table S5) (Ding *et al.*, 2020). Up-regulated genes shared by PTI and 'PTI+ETI' were mostly enriched in GO as defence-related genes or stress-response genes (Supplementary Fig. S6E, G), whereas down-regulated genes shared by both immune activation conditions were enriched with respect to genes involved in photosynthesis (Supplementary Fig. S6F, H). These results indicate a transcriptional reprogramming from photosynthesis to defence activation in Arabidopsis leaves upon activation of both immune conditions. In addition, we identified 3005 genes that were more strongly induced by 'PTI+ETI' than by PTI alone; they were distributed in Clusters 5, 7, and 9 based on their co-expression pattern (Supplementary Fig. S6D, I–K).

We hypothesized that rapid increase of gene expression would be correlated with increased chromatin accessibility at these gene loci during immune activation, as active transcription usually requires increased access by DNA-binding proteins such as TFs and transcriptional machinery (Klemm *et al.*, 2019). To test this hypothesis, we displayed ATAC-seq and corresponding RNA-seq data for well-known defence gene loci (Fig. 2). These genes were *ISOCHORISMATE SYNTHASE 1* (*ICS1*), *ENHANCED DISEASE SUSCEPTIBILITY 5* (*EDS5*), and *AVRPPHB SUSCEPTIBLE 3* (*PBS3*), genes involved in SA biosynthesis (Wildermuth *et al.*, 2001; Rekhter *et al.*, 2019; Torrens-Spence *et al.*, 2019; Ding and Ding, 2020), and *AGD2-LIKE DEFENSE RESPONSE PROTEIN 1* (*ALD1*), *SAR DEFICIENT 4* (*SARD4*), and *FLAVIN-DEPENDENT MONOOXYGENASE 1* (*FMO1*), genes involved in the synthesis of pipecolic acid and its derivatives,

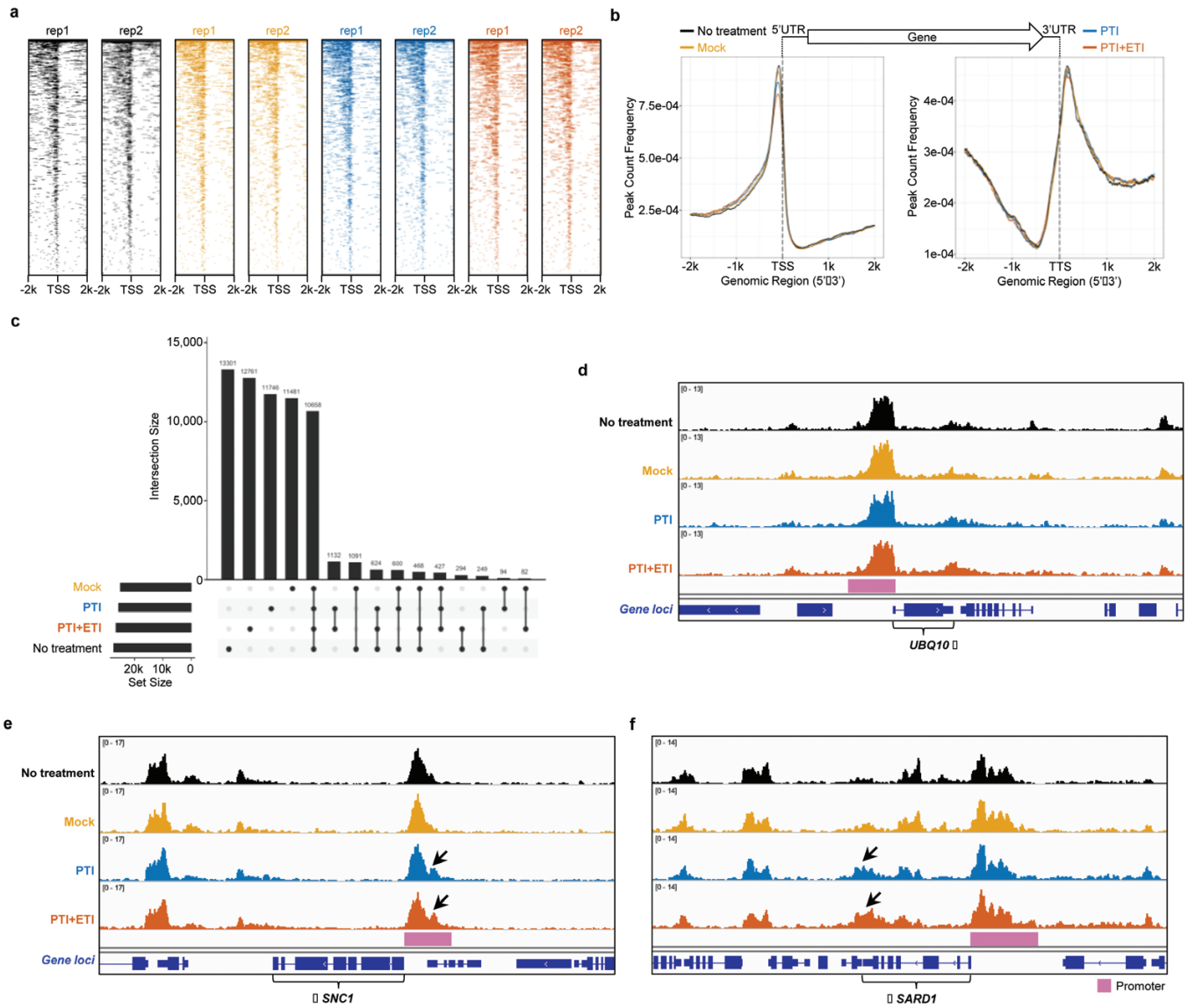

Fig. 1. Interrogation of chromatin landscapes activated by PTI and 'PTI+ETI'. (A) Heatmaps showing the distribution of accessible regions around the TSS identified by FANS-ATAC-seq in two biological replicates (rep) under four different conditions. Accessible regions are mapped to 2000 bp upstream (-2k) or downstream (2k) of the TSS (indicated at the centre). 'No treatment', Mock, PTI, and 'PTI+ETI' are indicated in black, orange, blue, and vermillion, respectively (the same colour codes apply to the same treatments in the rest of this study). (B) Distribution of accessible regions around the TSS (left panel) and TTS (right panel) identified from FANS-ATAC-seq with the mean peak counts from two biological replicates indicated in (A). The centre of accessible regions was used to produce the distribution plots. (C) An UpSet plot showing the relationships of accessible regions enriched under the four different conditions indicated in (A) and (B). 'Intersection size' indicates either condition-specific accessible regions or shared accessible regions under different combinations of condition comparisons. 'Set size' indicates the aggregates or total number of accessible regions found under each condition. (D–F) Genome browser views of ATAC-seq-indicated chromatin accessibility changes occurring near selected gene loci under different conditions. Gene symbols are labelled for the corresponding gene loci, (D) *UBQ10*, (E) *SNC1*, and (F) *SARD1*. The protein-coding strand is indicated by the black arrow placed next to the gene symbol. The pink bars next to each gene locus indicate their putative promoter regions.

which contribute to systemic acquired resistance and defence priming (Návarová *et al.*, 2012; Ding *et al.*, 2016; Hartmann *et al.*, 2018; Chen *et al.*, 2018). We observed strongly increased ACRs at the promoters of all six selected genes in PTI and 'PTI+ETI' compared with 'No treatment' or mock treatments (Fig. 2A–F), and increased transcripts of those genes (Fig. 2G–I). This indicates a positive correlation between rapid transcriptional up-regulation of selected defence genes and increased ACRs near the corresponding gene loci during activation of PTI and 'PTI+ETI'.

Genome-wide assessment of gene regulatory changes during ETI without PTI

Activation of ETI requires effector delivery from a pathogen, so will usually be preceded by PTI (except perhaps for some

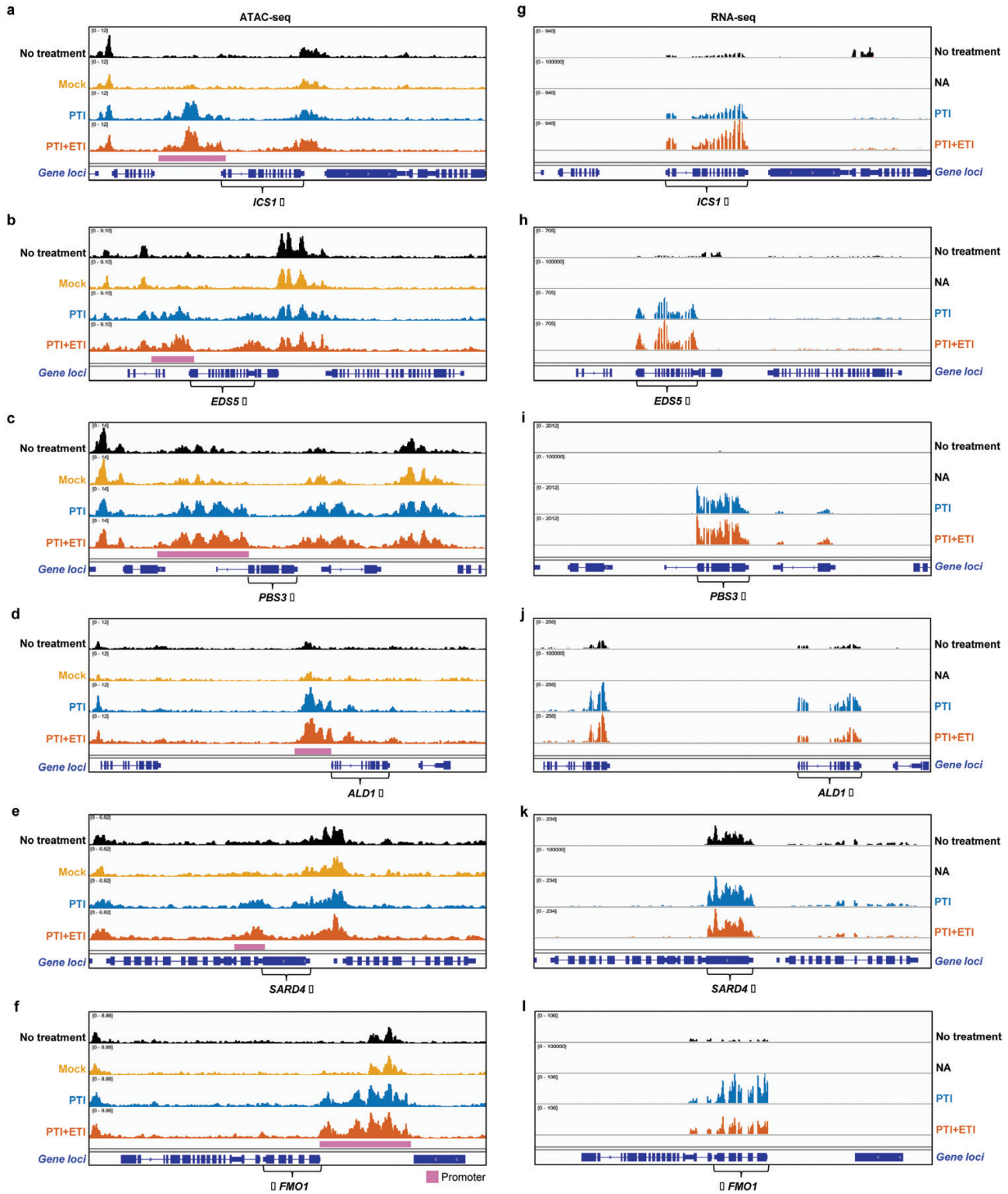

Fig. 2. Integration of ATAC-seq with RNA-seq for genes activated by PTI and 'PTI+ETI'. (A–F) and (G–I) Genome browser views of ATAC-seq and RNA-seq on indicated gene loci under different conditions. (A) and (G) are data for the *ICS1* locus; (B) and (H) are data for the *EDS5* locus; (C) and (I) are data for the *PBS3* locus; (D) and (J) are data for the *ALD1* locus; (E) and (K) are data for the *SARD4* locus; (F) and (I) are data for the *FMO1* locus. *ICS1*, *EDS5*, and *PBS3* are genes encoding enzymes that are required for the biosynthesis of the defence hormone SA in the isochorismate pathway. *ALD1*, *SARD4*, and *FMO1* are genes encoding enzymes involved in the biosynthesis of the secondary metabolite *N*-hydroxypipecolic acid, which is required to initiate systemic acquired resistance in plants. ATAC-seq data contain the same four conditions as shown in Fig. 1, whereas the data point of the mock treatment is absent in the RNA-seq data (NA). ATAC-seq and RNA-seq data points with corresponding labels indicate that they were collected under exactly the same conditions (see the Materials and methods for more details).

recognized viruses). Previous studies on ETI usually involve effector delivery from *Pseudomonas* sp. or *Agrobacterium* transient expression, and thus are studies on 'PTI+ETI'. We previously reported an inducible ETI system by expressing AvrRps4^{WT} (SETI^{WT}), in which AvrRps4^{WT} is expressed only upon β-estradiol (E2)-induced nuclear binding of XVE to the LexA operon (E2:AvrRps4^{WT}) (Ngou *et al.*, 2020). This system enables investigation of ETI-specific physiological changes (Ngou *et al.*, 2021).

ETI induced in SETI^{WT} displays similar transcriptional dynamics to those induced by Pf0-1 EtHAn (Ngou *et al.*, 2020). We focused on ETI-specific transcriptional activation; all RNA-seq samples were collected at a relatively early time point of the activation (4 hpi of E2) (Supplementary Fig. S7A) (Ngou et al., 2020, 2021). To obtain the list of DEGs during ETI, we compared gene expression profiles in E2-treated SETI^{WT} at 4 hpi (ETI) with those in E2-treated SETI^{WT} at 0 hpi (Control_1) or to those in E2-treated SETI^{mut} at 4 hpi (ETI_mut) (Supplementary Fig. S7A–D, Supplementary Tables S6, S7). The comparisons of 'ETI vs Control_1' and 'ETI vs ETI_mut' shared mostly the same genes in both the up- and down-regulated groups (1584 shared up-regulated and 1869 shared down-regulated genes, respectively) (Supplementary Fig. S7B–D). The number of DEGs in 'ETI vs Control_1' was much larger than that in 'ETI vs ETI_mut' (Supplementary Fig. S7B, D). The majority of up- and down-regulated DEGs in 'ETI vs ETI_mut' were shared by 'ETI vs Control_1' (Supplementary Fig. S7C, Supplementary Table S6). From the GO enrichment analysis of DEGs in those comparisons, we found that the GO term 'response to wounding' was enriched in DEGs of 'ETI vs Control_1' but not in that of 'ETI vs ETI_mut' (Supplementary Fig. S7E–H). This indicates that both ETI and ETI_mut activate genes that are induced by mechanical wounding via the infiltration process at 4 hpi. Thus, comparing ETI to ETI_mut in 'ETI vs ETI_mut' eliminates wounding-induced genes, and reduces background. From these DEGs in 'ETI vs ETI_mut', we found genes mostly enriched in the GO terms 'response to chitin', 'protein phosphorylation', and 'defence response' (Supplementary Fig. S7I–K) (Ngou *et al.*, 2021).

To study the changes in accessible chromatin at the loci of DEGs, we performed FANS-ATAC-seq (Supplementary Fig. S8A). Instead of using E2 treatment at 0 hpi, we used a mock-treated sample at 4 hpi as a negative control, imitating the effects from wounding (Supplementary Fig. S8A). We observed consistent genomic distribution patterns of ACRs in all samples (Supplementary Fig. S8B–J, Supplementary Table S8). To demonstrate ACRs that are specifically induced by ETI compared with all control conditions, we checked the *ICS1* locus in comparison to the housekeeping gene *UBQ10* locus (Fig. 3A, B). We found that only ETI, and not the 'No treatment_1' control or mock treatment, induced DARs in the *ICS1* promoter and 3′UTR (Fig. 3A). In contrast, the *UBQ10* promoter and proximal region were accessible among all treatments (Fig. 3B); therefore, we named this type of open chromatin as constitutively accessible chromatin regions. This is consistent with the stable expression of *UBQ10* under all conditions.

Integration of ATAC-seq and RNA-seq results in PTI, ETI, and 'PTI+ETI'

To identify genome-wide DARs that are activated by PTI, ETI, and 'PTI+ETI', we normalized the ATAC peaks enriched in the PTI, ETI, and 'PTI+ETI' treatments compared with the corresponding control conditions (Supplementary Fig. S9A–C). We found that DARs became visible at the promoters of *ICS1* and *FMO1* as well as the NADPH oxidase-encoding gene *RbohD* in response to the activation of PTI, ETI, and 'PTI+ETI' (Fig. 4A), consistent with their up-regulated expression in these conditions (Supplementary Figs S6, S7) (Ngou *et al.*, 2021). We observed no DARs at the *BIK1* locus under

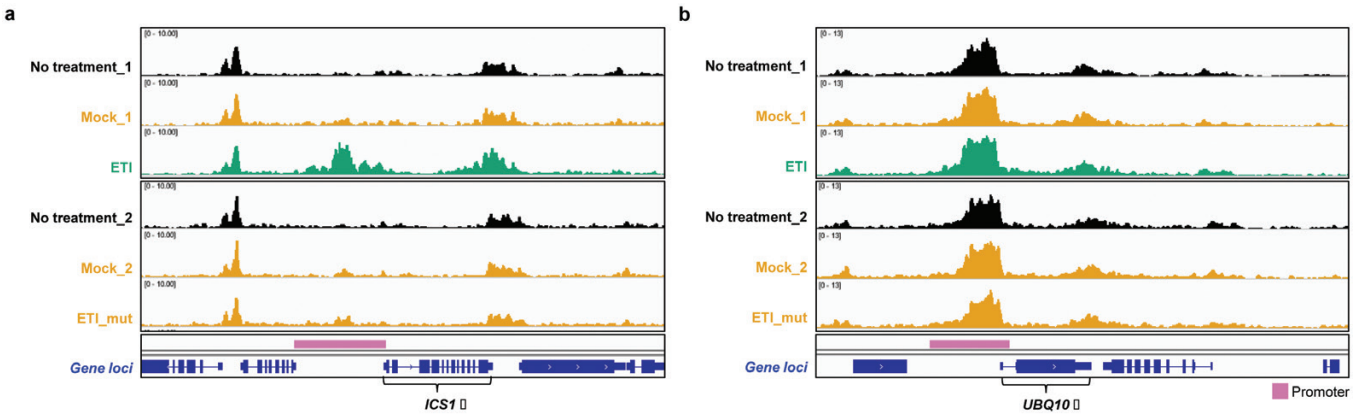

Fig. 3. Characterization of chromatin accessible regions activated by ETI. (A, Bb Genome browser views of chromatin accessible regions on selected gene loci under different conditions, including ETI. 'No treatment_1' and 'No treatment_2' are coloured in black. Mock_1, Mock_2 and ETI_mut are coloured in orange. ETI is coloured in bluish green. The same colour codes apply to the corresponding conditions in the rest of this study. The gene loci are labelled with their corresponding gene names, (A) *ICS1* and (B) *UBQ10*. The protein-coding strand is indicated with a black arrow next to the gene name. The pink bars next to each gene locus indicate their putative promoter regions.

PTI, ETI, or 'PTI+ETI' (Fig. 4B), although the expression of *BIK1* was induced in all these conditions (Supplementary Figs S6, S7) (Ngou *et al.*, 2021). In addition, we observed that DARs at *PEP1 RECEPTOR 2* (*PEPR2*) and *SARD1* loci were significantly induced only by ETI (Fig. 4B), but the expression of these genes was induced under all immune activation conditions (Supplementary Figs S6, S7) (Ngou *et al.*, 2021). This indicates that not all increased DARs activated by different immune systems are positively associated with the up-regulated expression of their respective genes.

To determine the extent to which activated open chromatin regions from the ATAC-seq analysis are correlated with induced gene expression in all immune conditions, we integrated our ATAC-seq data with corresponding RNA-seq data. We found 1646 gene loci with increased ATAC peaks (DARs) as well as significantly up-regulated gene expression (DEGs) in PTI versus 'No treatment', and 1722 such loci in 'PTI+ETI' versus 'No treatment' (Fig. 4C, Supplementary Table S9). By comparing the intersection of the positively correlated gene loci ('DAR∩DEG'), we found substantial overlap (1413 gene loci) between these two conditions (Fig. 4C, Supplementary Table S9). Comparing 'ETI vs Mock', we found 947 loci showing positive correlation of increased DARs and up-regulated DEGs (Fig. 4D, Supplementary Table S9). The same GO terms were enriched in both 1413 and 947 loci lists (Fig. 4C, Supplementary Fig. S9C, D, Supplementary Table S9). Thus, a common set of genes is activated during PTI, ETI, and 'PTI+ETI', and transcriptional activation might require chromatin in these gene loci to open up for active transcription events.

To better understand the correlation between DEGs and DARs that are induced by PTI, ETI, and 'PTI+ETI', we individually compared up-regulated DEGs, DARs, and 'DAR∩DEG' that are activated in these conditions compared with the corresponding control conditions (Fig. 4E–G, Supplementary Table S9). We found that a large proportion of both up-regulated genes and increased DARs were shared by all three immune activation conditions (Fig. 4E, F, Supplementary Table S9). We then compared PTI, ETI, and 'PTI+ETI' up-regulated DEGs and DARs ('DAR∩DEG'), and identified 652 gene loci shared by PTI, ETI, and 'PTI+ETI' (Fig. 4G, Supplementary Table S9). These responses shared by PTI, ETI, and 'PTI+ETI' could reveal a common transcriptional regulatory mechanism, in which a common set of TFs might be required for controlling gene expression.

Transcriptional GRNs of PTI, ETI, and 'PTI+ETI'

Identification of ACRs can assist in determining the locations of putative *cis*-regulatory elements, where transcriptional regulators, especially DNA-binding proteins such as TFs, might bind. To identify regulatory interactions between TF regulators and target genes, GRNs were delineated through the integration of RNA-Seq, ATAC-Seq, and TF motif information (Kulkarni *et al.*, 2018). GRNs at an early time point (4 hpi) upon activation of PTI, ETI, and 'PTI+ETI' were constructed, based on motifs enriched for DARs in these conditions. TF binding site mapping data for 1793 motifs, corresponding to 916 Arabidopsis TFs, were used to link specific regulators with putative target genes, based on the motif location in the DAR and the closest gene (Kulkarni *et al.*, 2018). To narrow down the list of TFs, we selected those that showed increased gene expression ($\log_2$FC>1, q-value<0.01; Supplementary Table S10). We identified 115, 34, and 133 TFs as regulators in PTI, ETI, and 'PTI+ETI', based on the significant enrichment of 210, 73, and 248 motifs in the corresponding DARs (Fig. 5A, Supplementary Table S10). Comparing regulators between the different conditions revealed that 25 regulators, of which 72% are WRKY TFs, are common to all three networks, while 82 regulators are shared between PTI and 'PTI+ETI', corresponding predominantly with WRKY, bHLH, and bZIP TFs (Fig. 5B). This result reveals that a diversity of TF families plays an important role in the transcriptional reprogramming of gene expression during the activation of plant immunity.

To assess the biological processes controlled by these different regulators, GO enrichment was performed on each set of target genes, per network and per TF. We found that 'response to chitin', 'response to bacterium', and 'response to hypoxia' were the top three GO terms that are commonly enriched in PTI, ETI, and 'PTI+ETI' (Fig. 5C, Supplementary Fig. S10, Supplementary Table S10). Whereas most WRKYs are activated during immune responses independently of whether the activation occurs through surface or intracellular receptors, WRKY65 and WRKY59 are specific to ETI, and the targets of WRKY59 are enriched in 'regulation of cell death' (Fig. 6, Supplementary Fig. S10B). Some examples of TFs implicated by this analysis, some of which have been confirmed in controlling hormone-related processes, are: (i) response to JA and SA in PTI: AtIDD5; (ii) response to SA in PTI: KAN2, WRKY33, WRKY45, TGA7, and JKD; (iii) SA signaling in ETI: AT5G01380; and (iv) response to SA in 'PTI+ETI': KAN2, ANAC029, ANAC046, ABO3, TGA3, and TGA7 (Supplementary Fig. S10). Response to abscisic acid was observed for only eight WRKY TFs in PTI (WRKY7, 11, 15, 17, 22, 40, 45, and 75), which might be mostly associated with the wounding response. Stronger induction of ETI in addition to PTI might be more dominant to this abscisic acid- or wounding-associated transcriptional regulation. Two members of the CAMTA TF family (CAMTA1 and CAMTA3) were exclusively enriched in ETI and were previously characterized as repressors of SA-regulated genes. However, upon pathogen infection, CAMTA-mediated repression is alleviated and plant defence genes are expressed (Kidokoro *et al.*, 2017; Kim *et al.*, 2017; Yuan *et al.*, 2018). These results indicate that the functions of these CAMTA TFs involved in immunity are mediated by intracellular receptors. For PTI, there was only one TF exclusive to this condition, CBF2, which regulates a PTI-specific GO term, 'toxin metabolic process'.

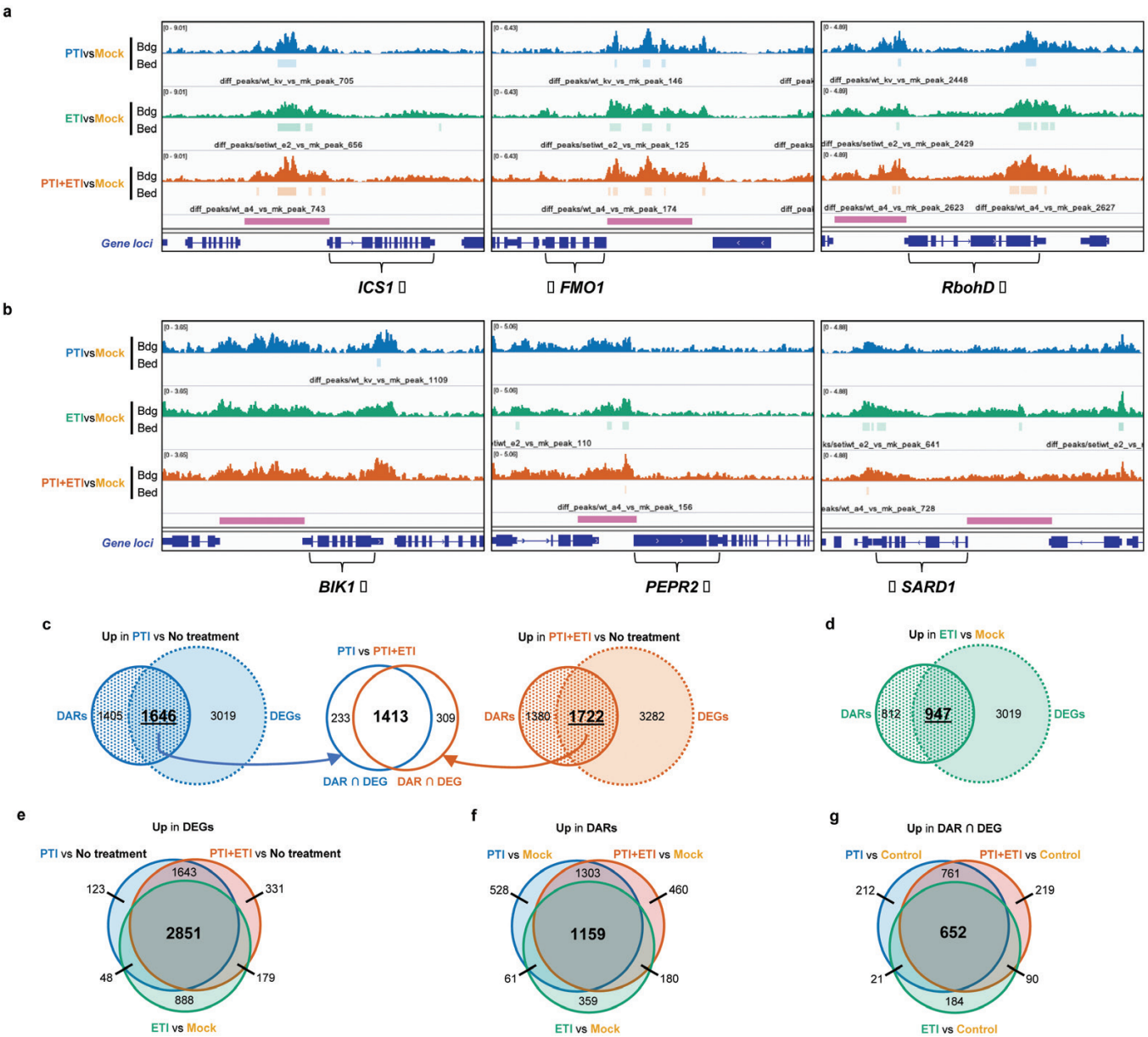

Fig. 4. Determining chromatin accessibility changes and changes in gene expression activated by PTI, ETI, and 'PTI+ETI'. (A, B) Genome browser views of differentially accessible chromatin regions (ACRs) near genes that are transcriptionally up-regulated in PTI, ETI, and 'PTI+ETI' compared with treatments. 'Bdg' stands for the extension of the data loaded in the genome browser as the Badge Designer 2000 Photo ID format; 'Bed' stands for the extension of the data loaded in the genome browser as the Browser Extensible Data format. (A) Gene loci (*ICS1*, *FMO1*, and *RbohD*) with increased ACRs in all indicated conditions. (B) Gene loci that either have no increased ACRs in all conditions (*BIK1*) or show increased ACRs in only ETI (*PEPR2* and *SARD1*). Other labels follow the same keys indicated in Figs 1–3. (C) Integration of DARs and DEGs between PTI and 'PTI+ETI'. The DARs indicate the nearest gene loci. The Venn diagrams on the left or right sides show up-regulated DARs (circle with dotted colour filling) and DEGs (dashed circle with solid colour filling) in PTI (blue, left) or 'PTI+ETI' (vermillion, right) compared with 'No treatment' controls. Shared gene loci with both DARs and DEGs (the intersection area in the Venn diagrams, or 'DARnDEG') from PTI (n=1635) and 'PTI+ETI' (n=1722) were compared again in the Venn diagram in the middle. (D) Integration of DARs and DEGs in ETI. The Venn diagram shows up-regulated DARs (circle with dotted filling) and DEGs (dashed circle with solid filling) in ETI compared with Mock controls. (E) Comparisons of up-regulated DEGs in PTI, ETI, and 'PTI+ETI' compared with corresponding negative controls ('No treatment' or Mock). (F) Comparisons of up-regulated DARs in PTI, ETI, and 'PTI+ETI' compared with corresponding negative controls ('No treatment' or Mock). (G) Comparisons of up-regulated 'DARnDEG' in PTI, ETI, and 'PTI+ETI' compared with controls ('No treatment' or Mock).

The clustering coefficient of a network is a measure of the tendency of the nodes to cluster together, which for GRNs indicates that for specific genes, the incoming regulatory TFs are also controlling each other, suggesting TF crosstalk. The clustering coefficient was significantly higher for the PTI and ETI networks than for 'PTI+ETI' and the intersection

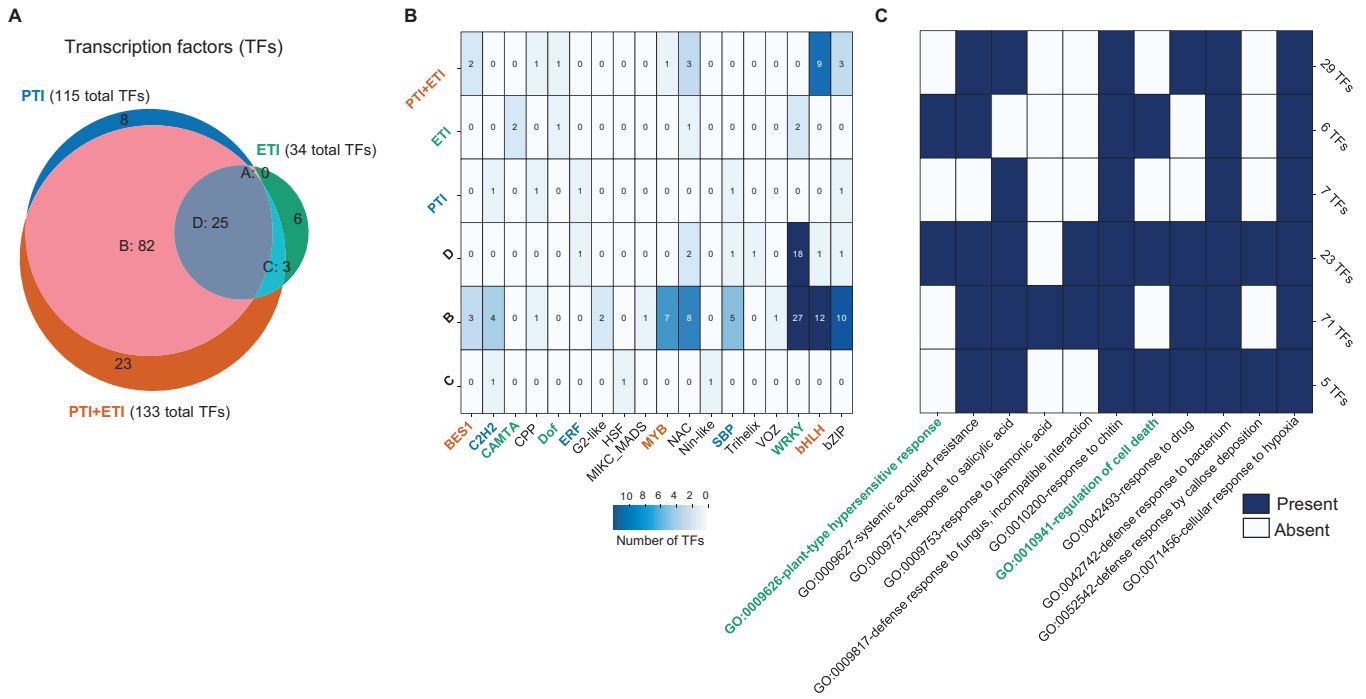

Fig. 5. Overview of regulatory TFs across the different gene regulatory networks. (A) Venn diagram showing shared and unique TFs across the different networks inferred for each condition. (B) Heatmap showing the number of TF family members in each of the Venn diagram sets shown in (A), as indicated by the colour of each cell. TFs that are specific to PTI, ETI, and 'PTI+ETI' are highlighted with the corresponding colour (blue, green, and vermilion, respectively). (C) Heatmap displaying the presence or absence of GO term enrichment in each of the Venn diagram sets. Numbers at the right indicate the number of TFs showing GO enrichment. TFs that are specific to ETI are enriched in 'plant-type hypersensitive response' and 'regulation of cell death' (in green).

of PTI, ETI, and 'PTI+ETI' (PTI∩ETI∩'PTI+ETI', or 'Set D'; Supplementary Fig. S11). The ETI network stands out in having 23 genes with a clustering coefficient of 0.5 or higher, which are controlled by a combination of WRKY TFs (WRKY6, 26, 31, 40, 47, and 70), CAMTA3, HSFB2A, and IDD1 (Supplementary Fig. S12). Overall, the inferred networks revealed that both shared and unique regulators are involved in controlling gene expression, with an important role for WRKY TFs in controlling the 'response to bacteria' as well as other TFs regulating other hormone-related biological processes. In addition, the tight control of specific target genes by multiple TFs, some also controlling each other, enables investigation into the hierarchy of TF signalling in different types of immune activation.

Discussion

Our understanding of transcriptional regulation in eukaryotes has been greatly advanced by the application of high-throughput sequencing methods to chromatin biology (Meyer and Liu, 2014). Genome-wide chromatin accessibility data for different plant species have demonstrated interesting aspects of mechanisms involved in the transcriptional regulation of diverse biological processes (Maher *et al.*, 2018; Potter *et al.*, 2018; Sijacic *et al.*, 2018; Frerichs *et al.*, 2019; Lu *et al.*, 2019; Ricci *et al.*, 2019), but rarely for plant immunity. Several TFs have been implicated in plant innate immunity (Tsuda and Somssich, 2015; Garner *et al.*, 2016). How these TFs function in a regulatory network has remained poorly understood. Here, we report chromatin accessibility landscapes that are activated by both cell-surface and intracellular immune receptor-mediated immunity (i.e. PTI and ETI) (Figs 1, 3). There are few studies of ETI in the absence of PTI, and we highlight here the similarities and differences in terms of changes in chromatin accessibility and associated gene expression between these two systems. For those who are interested in PTI or ETI, these datasets comprise a valuable resource for identifying potential novel regulatory components. In addition, these comparative studies document for the first time the similarities and differences among PTI, ETI, and 'PTI+ETI', directly demonstrating the interactive relationship between the cell-surface and intracellular immune systems at the transcriptional level.

From the minimum GRNs we constructed here based on our ATAC-seq and RNA-seq results after filtering with selected GO terms, we show that WRKY TFs are the predominant players in the GRNs regulating most genes that are activated during both PTI and ETI (Fig. 6, Supplementary Fig. S12). However, due to incomplete public data, our GRNs reported here cannot reflect all regulatory possibilities. For instance, the DNA-binding motifs of some TFs are still not known (O'Malley *et al.*, 2016). In addition, we prioritized

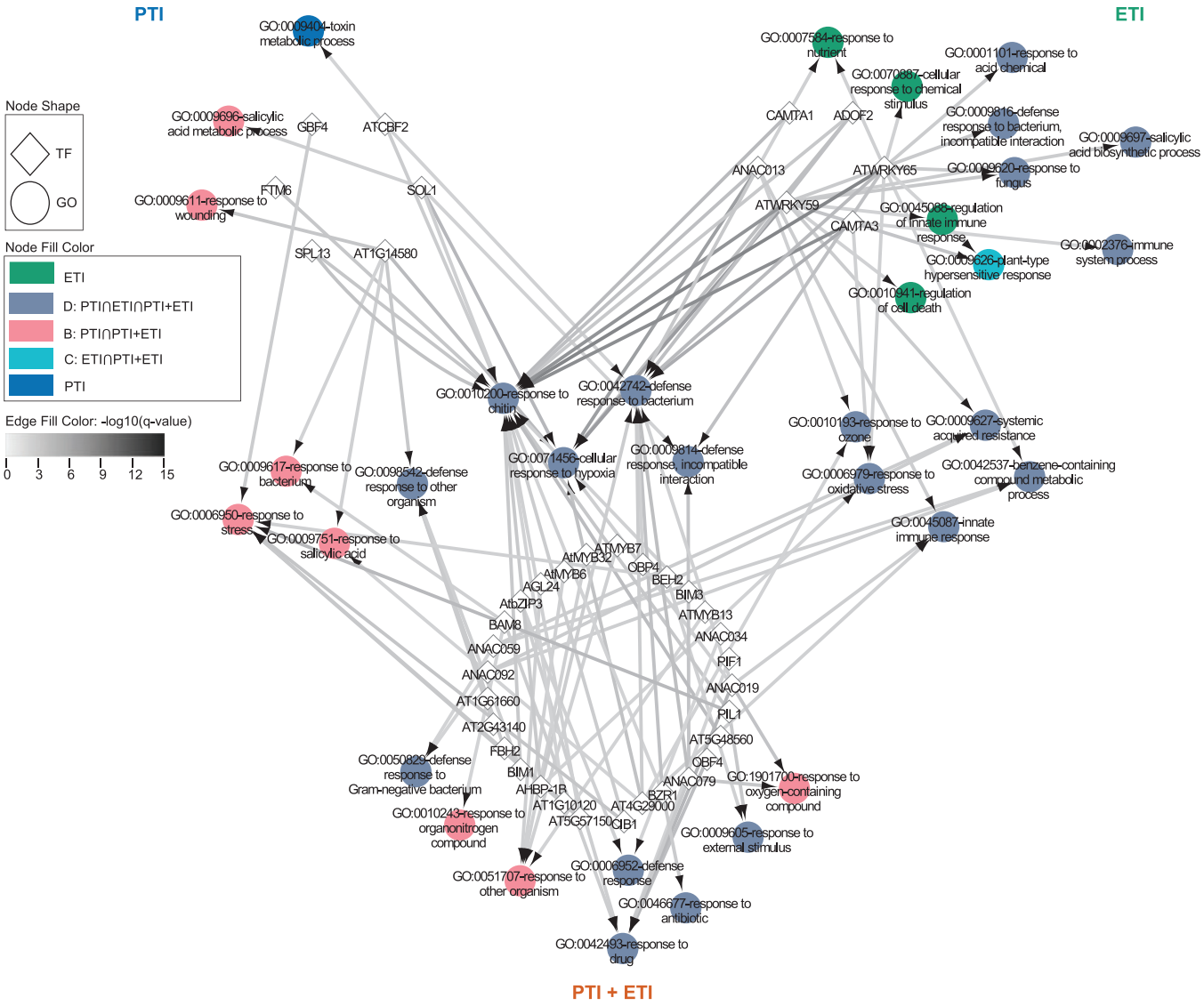

Fig. 6. TF-GO term network for condition-specific TFs. Network diagram with the TFs specific for each condition, PTI, ETI, and 'PTI+ETI', organized in circles linked to the GO terms enriched in the putative target genes they control. The GO terms are coloured according to whether they are exclusive to any specific condition or belong in any of the possible intersections of the conditions (as indicated by the colour key). The GO terms controlled by TFs exclusive to one condition are in the outermost parts. The GO terms controlled by TFs exclusive to two or three conditions are located closer to the centre and in the centre, respectively. Note that there are no GO terms shared between TFs of PTI and ETI. In addition, there are no GO terms that are exclusive to 'PTI+ETI' or 'PTI∩ETI' because none of them are controlled by PTI, ETI, or 'PTI+ETI' exclusive TFs.

up-regulated genes in our analysis, and negative regulation of some genes upon TF binding might also play an important role. These networks will be further improved when more data become available.

Another important area of uncertainty is the link between the recruitment of TFs to defence gene promoters and changes in chromatin accessibility. Several working models have been proposed in which remodelling of chromatin accessibility is led by the TFs (Klemm *et al.*, 2019). For up-regulated DEGs that show increased DARs, the binding of TFs might be correlated with chromatin opening. However, it is challenging to distinguish whether TF binding is a cause or a consequence of chromatin opening. Some TFs can serve as 'pioneer' TFs to initiate transcription by recruiting 'non-pioneer' TFs, other transcriptional regulators, and the RNA polymerase II machinery (Meyer and Liu, 2014; Soufi *et al.*, 2015; Jin *et al.*, 2021). Such 'pioneer' TFs may recruit components that can open the chromatin, such as histone remodellers (Meyer and Liu, 2014). However, more genetic evidence is required to evaluate this hypothesis.

The chromatin accessibility landscapes and implied GRNs reported here provide a snapshot of events during the activation of different immune responses. Transcription, like many other processes, is dynamic, so it is important to profile the changes

in chromatin accessibility and corresponding gene expression over a time-course. For instance, our PTI ATAC-seq data were collected at 4 hpi, but PTI-induced transcriptional reprogramming occurs as early as within first the 30 min after PTI activation (Bjornson *et al.*, 2021); therefore, it is uncertain whether the changes in chromatin accessibility induced by PTI are the cause or the effect of the PTI-induced transcriptional changes. With time-series ATAC-seq and RNA-seq data obtained in future studies, we will be able to generate dynamic transcriptional regulatory networks that will provide more insights into the transcriptional regulatory mechanisms required for immune activation and for the establishment of disease resistance. Overall, the tools we provide here can also be broadly applied to analyse ATAC-seq and RNA-seq datasets generated from studying any inducible or developmentally regulated system. The network analysis, conducted here with Arabidopsis, can also be compared to network analyses with other plant species when their ATAC-seq and RNA-seq datasets are available, enabling evolutionary comparisons of GRNs across plant species.

Supplementary data

The following supplementary data are available at *JXB* online.

Fig. S1. Schematic view of integrated plant innate immune system.

Fig. S2. Establishment of FANS-ATAC-seq for Arabidopsis leaf tissue.

Fig. S3. Trial run results of FANS-ATAC-seq for Arabidopsis leaf tissue demonstrate a good reproducibility.

Fig. S4. FANS-ATAC-seq using Arabidopsis leaf nuclei and vegetative and sperm nuclei derived from Arabidopsis pollen grains show tissue-specific chromatin accessibility.

Fig. S5. Additional information of FANS-ATAC-seq for chromatin landscapes activated by PTI and 'PTI+ETI'.

Fig. S6. RNA-seq implies differential gene expression during the activation of PTI and 'PTI+ETI'.

Fig. S7. RNA-seq implies differential gene expression during the activation of ETI.

Fig. S8. Interrogation of chromatin landscapes activated by ETI.

Fig. S9. Normalization of accessible chromatin regions for DARs and related GO enrichment.

Fig. S10. TF target gene GO enrichment heatmaps.

Fig. S11. Network centrality parameters.

Fig. S12. ETI network for targets with high clustering coefficient.

Table S1. Dual index primers for multiplexing; associated with Supplementary Figs S2 and S3.

Table S2. Distribution of enriched accessible chromatins on different genomic features under different treatments in Supplementary Fig.5.

Table S3. Accessible chromatin regions enriched in different treatment groups and intersections between groups in Fig. 1C.

Table S4. Statistics of differentially expressed genes listed in Supplementary Fig. 6C.

Table S5. Expression value and cluster information of genes listed in Supplementary Fig. 6D.

Table S6. Statistics of differentially expressed genes listed in Supplementary Fig. 7C.

Table S7. Expression value and cluster information of genes listed in Supplementary Fig. 7D.

Table S8. Distribution of enriched accessible chromatins on different genomic features under different treatments in Supplementary Fig. 8.

Table S9. Gene lists and their GO terms enriched in DARs and DEGs data integration, related to Fig. 4 and Supplementary Fig. 9.

Table S10. Information for gene regulatory networks learned from ATAC-seq and RNA-seq under different immune conditions, related to Figs 5 and 6 and Supplementary Figs S10–S12.

Acknowledgements

We thank the Gatsby Foundation (UK) for funding to the JDGJ laboratory. PD acknowledges support from the European Union's Horizon 2020 Research and Innovation Program under Marie Skłodowska-Curie Actions (grant agreement: 656243) and a Future Leader Fellowship from the Biotechnology and Biological Sciences Research Council (BBSRC) (grant agreement: BB/R012172/1). TS, RKS, DM, and JDGJ were supported by the Gatsby Foundation funding to the Sainsbury Laboratory. NMP and KV were supported by a BOF grant from Ghent University (grant agreement: BOF24Y2019001901). WG and RZ were supported by the Scottish Government Rural and Environment Science and Analytical Services division (RESAS), and RZ also acknowledges the support from a BBSRC Bioinformatics and Biological Resources Fund (grant agreement: BB/S020160/1). BPMN was supported by the Norwich Research Park (NRP) Biosciences Doctoral Training Partnership (DTP) funded by the BBSRC (grant agreement: BB/M011216/1). SH and XF were supported by a BBSRC Responsive Mode grant (grant agreement: BB/S009620/1) and a European Research Council Starting grant 'SexMeth' (grant agreement: 804981). CL was supported by Deutsche Forschungsgemeinschaft (grant agreement: LI 2862/4).

Author contributions

PD and JDGJ conceptualized and designed the research; PD conducted all experiments with assistance from BPMN and SH; PD together with TS, RKS, NMP, WG, and CL performed data analyses, with assistance from DM, RZ, and KV. PD wrote the manuscript with input from all co-authors; all authors helped with editing and finalizing the manuscript.

Conflict of interest

The authors declare no competing interests.

Data availability

All raw reads in this study have been uploaded to the European Nucleotide Archive (ENA) data repository (https://www.ebi.ac.uk/ena/browser/

home) and can be retrieved through accession numbers PRJEB34955 and PRJEB38924 for RNA-seq and PRJEB38923 for ATAC-seq. For data reproducibility, all scripts generated in this study and software versions can be accessed via the GitHub links indicated in the Materials and methods. All other data supporting the findings of this study are available within the paper and within its supplementary materials published online.

References

Asai S, Furzer OJ, Cevik V, Kim DS, Ishaque N, Goritschnig S, Staskawicz BJ, Shirasu K, Jones JDG. 2018. A downy mildew effector evades recognition by polymorphism of expression and subcellular localization. Nature Communications **9**, 5192.

Bacete L, Mélida H, Miedes E, Molina A. 2018. Plant cell wall-mediated immunity: cell wall changes trigger disease resistance responses. The Plant Journal **93**, 614–636.

Berriri S, Gangappa SN, Kumar SV. 2016. SWR1 chromatin-remodeling complex subunits and H2A.Z have non-overlapping functions in immunity and gene regulation in *Arabidopsis*. Molecular Plant **9**, 1051–1065.

Bjornson M, Pimprikar P, Nürnberger T, Zipfel C. 2021. The transcriptional landscape of *Arabidopsis thaliana* pattern-triggered immunity. Nature Plants **7**, 579–586.

Bray NL, Pimentel H, Melsted P, Pachter L. 2016. Near-optimal probabilistic RNA-seq quantification. Nature Biotechnology **34**, 525–527.

Buenrostro JD, Giresi PG, Zaba LC, Chang HY, Greenleaf WJ. 2013. Transposition of native chromatin for fast and sensitive epigenomic profiling of open chromatin, DNA-binding proteins and nucleosome position. Nature Methods **10**, 1213–1218.

Buenrostro JD, Wu B, Chang HY, Greenleaf WJ. 2015. ATAC-seq: a method for assaying chromatin accessibility genome-wide. Current Protocols in Molecular Biology **109**, 21.29.1–21.29.9.

Chen W, Zhu Q, Liu Y, Zhang Q. 2017. Chromatin remodeling and plant immunity. Advances in Protein Chemistry and Structural Biology **106**, 243–260.

Chen YC, Holmes EC, Rajniak J, Kim JG, Tang S, Fischer CR, Mudgett MB, Sattely ES. 2018. *N*-hydroxy-pipecolic acid is a mobile metabolite that induces systemic disease resistance in *Arabidopsis*. Proceedings of the National Academy of Sciences, USA **115**, E4920–E4929.

Choi HW, Klessig DF. 2016. DAMPs, MAMPs, and NAMPs in plant innate immunity. BMC Plant Biology **16**, 232.

Conway JR, Lex A, Gehlenborg N. 2017. UpSetR: an R package for the visualization of intersecting sets and their properties. Bioinformatics **33**, 2938–2940.

Ding P, Ding Y. 2020. Stories of salicylic acid: a plant defense hormone. Trends in Plant Science **25**, 549–565.

Ding P, Ngou BPM, Furzer OJ, Sakai T, Shrestha RK, MacLean D, Jones JDG. 2020. High-resolution expression profiling of selected gene sets during plant immune activation. Plant Biotechnology Journal **18**, 1610–1619.

Ding P, Rekhter D, Ding Y, *et al.* 2016. Characterization of a pipecolic acid biosynthesis pathway required for systemic acquired resistance. The Plant Cell **28**, 2603–2615.

Dong OX, Ao K, Xu F, *et al.* 2018. Individual components of paired typical NLR immune receptors are regulated by distinct E3 ligases. Nature Plants **4**, 699–710.

Frerichs A, Engelhorn J, Altmüller J, Gutierrez-Marcos J, Werr W. 2019. Specific chromatin changes mark lateral organ founder cells in the Arabidopsis inflorescence meristem. Journal of Experimental Botany **70**, 3867–3879.

Frith MC, Li MC, Weng Z. 2003. Cluster-Buster: finding dense clusters of motifs in DNA sequences. Nucleic Acids Research **31**, 3666–3668.

Garner CM, Kim SH, Spears BJ, Gassmann W. 2016. Express yourself: transcriptional regulation of plant innate immunity. Seminars in Cell & Developmental Biology **56**, 150–162.

Grant CE, Bailey TL, Noble WS. 2011. FIMO: scanning for occurrences of a given motif. Bioinformatics **27**, 1017–1018.

Guo W, Tzioutziou NA, Stephen G, Milne I, Calixto CP, Waugh R, Brown JWS, Zhang R. 2020. 3D RNA-seq: a powerful and flexible tool for rapid and accurate differential expression and alternative splicing analysis of RNA-seq data for biologists. RNA Biology doi: 10.1080/15476286.2020.1858253

Hammond-Kosack KE, Jones JD. 1997. Plant disease resistance genes. Annual Review of Plant Physiology and Plant Molecular Biology **48**, 575–607.

Hartmann M, Zeier T, Bernsdorff F, *et al.* 2018. Flavin monooxygenase-generated N-hydroxypipecolic acid is a critical element of plant systemic immunity. Cell **173**, 456–469.e16.

Hillmer RA, Tsuda K, Rallapalli G, Asai S, Truman W, Papke MD, Sakakibara H, Jones JDG, Myers CL, Katagiri F. 2017. The highly buffered Arabidopsis immune signaling network conceals the functions of its components. PLoS Genetics **13**, e1006639.

Jin R, Klasfeld S, Garcia MF, Xiao J, Han S-K, Konkol A, Zhu Y, Wagner D. 2021. LEAFY is a pioneer transcription factor and licenses cell reprogramming to floral fate. Nature Communications **12**, 626.

Johnson KC, Xia S, Feng X, Li X. 2015. The chromatin remodeler SPLAYED negatively regulates SNC1-mediated immunity. Plant & Cell Physiology **56**, 1616–1623.

Jones JD, Dangl JL. 2006. The plant immune system. Nature **444**, 323–329.

Kidd BN, Edgar CI, Kumar KK, Aitken EA, Schenk PM, Manners JM, Kazan K. 2009. The Mediator complex subunit PFT1 is a key regulator of jasmonate-dependent defense in *Arabidopsis*. The Plant Cell **21**, 2237–2252.

Kidokoro S, Yoneda K, Takasaki H, Takahashi F, Shinozaki K, Yamaguchi-Shinozaki K. 2017. Different cold-signaling pathways function in the responses to rapid and gradual decreases in temperature. The Plant Cell **29**, 760–774.

Kim D, Pertea G, Trapnell C, Pimentel H, Kelley R, Salzberg SL. 2013. TopHat2: accurate alignment of transcriptomes in the presence of insertions, deletions and gene fusions. Genome Biology **14**, R36.

Kim YS, An C, Park S, Gilmour SJ, Wang L, Renna L, Brandizzi F, Grumet R, Thomashow MF. 2017. CAMTA-mediated regulation of salicylic acid immunity pathway genes in Arabidopsis exposed to low temperature and pathogen infection. The Plant Cell **29**, 2465–2477.

Klemm SL, Shipony Z, Greenleaf WJ. 2019. Chromatin accessibility and the regulatory epigenome. Nature Reviews. Genetics **20**, 207–220.

Kulkarni SR, Jones DM, Vandepoele K. 2019. Enhanced maps of transcription factor binding sites improve regulatory networks learned from accessible chromatin data. Plant Physiology **181**, 412–425.

Kulkarni SR, Vaneechoutte D, Van de Velde J, Vandepoele K. 2018. TF2Network: predicting transcription factor regulators and gene regulatory networks in Arabidopsis using publicly available binding site information. Nucleic Acids Research **46**, e31.

Langmead B, Salzberg SL. 2012. Fast gapped-read alignment with Bowtie 2. Nature Methods **9**, 357–359.

Law CW, Chen Y, Shi W, Smyth GK. 2014. voom: precision weights unlock linear model analysis tools for RNA-seq read counts. Genome Biology **15**, R29.

Li B, Meng X, Shan L, He P. 2016. Transcriptional regulation of pattern-triggered immunity in plants. Cell Host & Microbe **19**, 641–650.

Li H, Handsaker B, Wysoker A, Fennell T, Ruan J, Homer N, Marth G, Abecasis G, Durbin R, 1000 Genome Project Data Processing Subgroup. 2009. The Sequence Alignment/Map format and SAMtools. Bioinformatics **25**, 2078–2079.

Lu Z, Hofmeister BT, Vollmers C, DuBois RM, Schmitz RJ. 2017. Combining ATAC-seq with nuclei sorting for discovery of cis-regulatory regions in plant genomes. Nucleic Acids Research **45**, e41.

Lu Z, Marand AP, Ricci WA, Ethridge CL, Zhang X, Schmitz RJ. 2019. The prevalence, evolution and chromatin signatures of plant regulatory elements. Nature Plants **5**, 1250–1259.

Maher KA, Bajic M, Kajala K, *et al.* 2018. Profiling of accessible chromatin regions across multiple plant species and cell types reveals common gene regulatory principles and new control modules. The Plant Cell **30**, 15–36.

Meyer CA, Liu XS. 2014. Identifying and mitigating bias in next-generation sequencing methods for chromatin biology. Nature Reviews. Genetics **15**, 709–721.

Návarová H, Bernsdorff F, Döring AC, Zeier J. 2012. Pipecolic acid, an endogenous mediator of defense amplification and priming, is a critical regulator of inducible plant immunity. The Plant Cell **24**, 5123–5141.

Ngou BPM, Ahn H-K, Ding P, Jones JDG. 2021. Mutual potentiation of plant immunity by cell-surface and intracellular receptors. Nature **592**, 110–115.

Ngou BPM, Ahn HK, Ding P, Redkar A, Brown H, Ma Y, Youles M, Tomlinson L, Jones JDG. 2020. Estradiol-inducible AvrRps4 expression reveals distinct properties of TIR-NLR-mediated effector-triggered immunity. Journal of Experimental Botany **71**, 2186–2197.

O'Malley RC, Huang SC, Song L, Lewsey MG, Bartlett A, Nery JR, Galli M, Gallavotti A, Ecker JR. 2016. Cistrome and epicistrome features shape the regulatory DNA landscape. Cell **165**, 1280–1292.

Patro R, Duggal G, Love MI, Irizarry RA, Kingsford C. 2017. Salmon provides fast and bias-aware quantification of transcript expression. Nature Methods **14**, 417–419.

Potter KC, Wang J, Schaller GE, Kieber JJ. 2018. Cytokinin modulates context-dependent chromatin accessibility through the type-B response regulators. Nature Plants **4**, 1102–1111.

Quinlan AR, Hall IM. 2010. BEDTools: a flexible suite of utilities for comparing genomic features. Bioinformatics **26**, 841–842.

Raudvere U, Kolberg L, Kuzmin I, Arak T, Adler P, Peterson H, Vilo J. 2019. g:Profiler: a web server for functional enrichment analysis and conversions of gene lists (2019 update). Nucleic Acids Research **47**, W191–W198.

Rekhter D, Lüdke D, Ding Y, Feussner K, Zienkiewicz K, Lipka V, Wiermer M, Zhang Y, Feussner I. 2019. Isochorismate-derived biosynthesis of the plant stress hormone salicylic acid. Science **365**, 498–502.

Ricci WA, Lu Z, Ji L, *et al.* 2019. Widespread long-range *cis*-regulatory elements in the maize genome. Nature Plants **5**, 1237–1249.

Risso D, Ngai J, Speed TP, Dudoit S. 2014. Normalization of RNA-seq data using factor analysis of control genes or samples. Nature Biotechnology **32**, 896–902.

Ritchie ME, Phipson B, Wu D, Hu Y, Law CW, Shi W, Smyth GK. 2015. limma powers differential expression analyses for RNA-sequencing and microarray studies. Nucleic Acids Research **43**, e47.

Robinson JT, Thorvaldsdóttir H, Winckler W, Guttman M, Lander ES, Getz G, Mesirov JP. 2011. Integrative genomics viewer. Nature Biotechnology **29**, 24–26.

Robinson MD, Oshlack A. 2010. A scaling normalization method for differential expression analysis of RNA-seq data. Genome Biology **11**, R25.

Saucet SB, Ma Y, Sarris PF, Furzer OJ, Sohn KH, Jones JD. 2015. Two linked pairs of *Arabidopsis TNL* resistance genes independently confer recognition of bacterial effector AvrRps4. Nature Communications **6**, 6338.

Schmid M, Davison TS, Henz SR, Pape UJ, Demar M, Vingron M, Schölkopf B, Weigel D, Lohmann JU. 2005. A gene expression map of *Arabidopsis thaliana* development. Nature Genetics **37**, 501–506.

Sijacic P, Bajic M, McKinney EC, Meagher RB, Deal RB. 2018. Changes in chromatin accessibility between Arabidopsis stem cells and mesophyll cells illuminate cell type-specific transcription factor networks. The Plant Journal **94**, 215–231.

Sohn KH, Segonzac C, Rallapalli G, Sarris PF, Woo JY, Williams SJ, Newman TE, Paek KH, Kobe B, Jones JD. 2014. The nuclear immune receptor *RPS4* is required for *RRS1SLH1*-dependent constitutive defense activation in *Arabidopsis thaliana*. PLoS Genetics **10**, e1004655.

Sohn KH, Zhang Y, Jones JD. 2009. The *Pseudomonas syringae* effector protein, AvrRPS4, requires *in planta* processing and the KRVY domain to function. The Plant Journal **57**, 1079–1091.

Soufi A, Garcia MF, Jaroszewicz A, Osman N, Pellegrini M, Zaret KS. 2015. Pioneer transcription factors target partial DNA motifs on nucleosomes to initiate reprogramming. Cell **161**, 555–568.

Staal J, Kaliff M, Dewaele E, Persson M, Dixelius C. 2008. *RLM3*, a TIR domain encoding gene involved in broad-range immunity of Arabidopsis to necrotrophic fungal pathogens. The Plant Journal **55**, 188–200.

Sun T, Zhang Y, Li Y, Zhang Q, Ding Y, Zhang Y. 2015. ChIP-seq reveals broad roles of SARD1 and CBP60g in regulating plant immunity. Nature Communications **6**, 10159.

Thomas WJ, Thireault CA, Kimbrel JA, Chang JH. 2009. Recombineering and stable integration of the *Pseudomonas syringae* pv. *syringae* 61 *hrp/hrc* cluster into the genome of the soil bacterium *Pseudomonas fluorescens* Pf0-1. The Plant Journal **60**, 919–928.

Torrens-Spence MP, Bobokalonova A, Carballo V, Glinkerman CM, Pluskal T, Shen A, Weng JK. 2019. PBS3 and EPS1 complete salicylic acid biosynthesis from isochorismate in *Arabidopsis*. Molecular Plant **12**, 1577–1586.

Tsompana M, Buck MJ. 2014. Chromatin accessibility: a window into the genome. Epigenetics & Chromatin **7**, 33.

Tsuda K, Somssich IE. 2015. Transcriptional networks in plant immunity. New Phytologist **206**, 932–947.

van der Biezen EA, Freddie CT, Kahn K, Parker JE, Jones JD. 2002. *Arabidopsis RPP4* is a member of the *RPP5* multigene family of TIR-NB-LRR genes and confers downy mildew resistance through multiple signalling components. The Plant Journal **29**, 439–451.

Walley JW, Rowe HC, Xiao Y, Chehab EW, Kliebenstein DJ, Wagner D, Dehesh K. 2008. The chromatin remodeler SPLAYED regulates specific stress signaling pathways. PLoS Pathogens **4**, e1000237.

Wang L, Tsuda K, Truman W, Sato M, Nguyen le V, Katagiri F, Glazebrook J. 2011. CBP60g and SARD1 play partially redundant critical roles in salicylic acid signaling. The Plant Journal **67**, 1029–1041.

Wildermuth MC, Dewdney J, Wu G, Ausubel FM. 2001. Isochorismate synthase is required to synthesize salicylic acid for plant defence. Nature **414**, 562–565.

Xia S, Cheng YT, Huang S, *et al.* 2013. Regulation of transcription of nucleotide-binding leucine-rich repeat-encoding genes *SNC1* and *RPP4* via H3K4 trimethylation. Plant Physiology **162**, 1694–1705.

Yu G, Wang L-G, He Q-Y. 2015. ChIPseeker: an R/Bioconductor package for ChIP peak annotation, comparison and visualization. Bioinformatics **31**, 2382–2383.

Yuan P, Du L, Poovaiah BW. 2018. Ca^{2+}/Calmodulin-dependent AtSR1/CAMTA3 plays critical roles in balancing plant growth and immunity. International Journal of Molecular Sciences **19**, 1764.

Zhang R, Calixto CPG, Marquez Y, *et al.* 2017. A high quality Arabidopsis transcriptome for accurate transcript-level analysis of alternative splicing. Nucleic Acids Research **45**, 5061–5073.

Zhang Y, Goritschnig S, Dong X, Li X. 2003. A gain-of-function mutation in a plant disease resistance gene leads to constitutive activation of downstream signal transduction pathways in *suppressor of npr1-1, constitutive 1*. The Plant Cell **15**, 2636–2646.

Zhang Y, Liu T, Meyer CA, *et al.* 2008. Model-based analysis of ChIP-Seq (MACS). Genome Biology **9**, R137.

Zhang Y, Xu S, Ding P, *et al.* 2010. Control of salicylic acid synthesis and systemic acquired resistance by two members of a plant-specific family of transcription factors. Proceedings of the National Academy of Sciences, USA **107**, 18220–18225.

Zhou C, Zhang L, Duan J, Miki B, Wu K. 2005. *HISTONE DEACETYLASE19* is involved in jasmonic acid and ethylene signaling of pathogen response in Arabidopsis. The Plant Cell **17**, 1196–1204.

Zhu Z, Xu F, Zhang Y, Cheng YT, Wiermer M, Li X, Zhang Y. 2010. Arabidopsis resistance protein SNC1 activates immune responses through association with a transcriptional corepressor. Proceedings of the National Academy of Sciences, USA **107**, 13960–13965.

Zou B, Sun Q, Zhang W, Ding Y, Yang DL, Shi Z, Hua J. 2017. The Arabidopsis chromatin-remodeling factor CHR5 regulates plant immune responses and nucleosome occupancy. Plant & Cell Physiology **58**, 2202–2216.